Comprehensive variability analysis of blazars using *Fermi* light curves across multiple timescales

Zahir Shah,[1,*] Athar A. Dar,[1,2] Sikandar Akbar,[2,†] Anjum Peer,[3] Zahoor Malik,[4] Aaqib Manzoor,[5] Sajad Ahanger,[2] Javaid Tantry,[2] Zeeshan Nazir,[1] Debanjan Bose,[1] and Mushtaq Magray[1]

[1]*Department of Physics, Central University of Kashmir, Ganderbal-191131, India*
[2]*Department of Physics, University of Kashmir, Srinagar-190006, India*
[3]*Department of Physics, Islamic University of Science and Technology, Awantipora-192122, India*
[4]*Department of Physics, National Institute of Technology, Srinagar-190006, India*
[5]*Indian Institute of Astrophysics, Bangalore, India*

(Received 6 March 2025; accepted 28 May 2025; published 30 June 2025)

In this study, we conducted a systematic analysis of long-term *Fermi*-LAT γ-ray data for a sample of blazars, including flat spectrum radio quasars (FSRQs), BL Lacertae objects (BL Lacs), and blazar candidates of unknown type (BCU), to investigate their γ-ray variability. We focused on light curves binned in three-day, seven-day, and 30-day intervals to assess the impact of binning on variability, using data with $TS > 4$ as a detection threshold. We calculated fractional variability (F_{var}) for each category and found that FSRQs exhibit higher mean variability compared to BL Lacs and BCUs, with BCUs displaying intermediate variability closer to BL Lacs. The Kolmogorov-Smirnov test on the variability distributions of FSRQs, BL Lacs, and BCUs indicates that FSRQs differ from both BL Lacs and BCUs, whereas BCUs are more similar to BL Lacs. The observed higher variability in FSRQs is likely linked to more powerful jets and accretion processes. The correlation between γ-ray flux and spectral index suggests a moderate positive correlation for BL Lacs and BCUs, indicating a "softer when brighter" behavior. FSRQs, however, displayed a mild anticorrelation, suggesting a tendency for these sources to become harder as their flux increases. Additionally, the analysis of flux distributions revealed log-normal behavior in many sources, consistent with multiplicative variability processes in blazar jets. Some sources exhibit bimodal distributions, implying transitions between distinct emission states. Moreover, binning effects the observed variability, with longer bins smoothing short-term fluctuations. The power spectral density (PSD) analysis suggested that FSRQs exhibit steeper slopes, reflecting structured variability, while BL Lacs display shallower slopes, dominated by stochastic processes. The absence of PSD breaks suggests no dominant characteristic timescale within the *Fermi* window. Spectral index distributions further highlight complexity, often requiring multicomponent models.

DOI: 10.1103/61tz-jk8c

I. INTRODUCTION

The *Fermi* Large Area Telescope [1] has revolutionized our understanding of the γ-ray variable sky. With its large field of view (covering 20% of the sky) and its ability to scan the entire sky in approximately 3 h, the LAT offers enhanced effective area and sensitivity. This continuous monitoring capability has made it an essential observatory for temporal and spectral studies in γ rays. Over more than ten years, the LAT has been instrumental in identifying and consistently tracking numerous variable celestial sources [2].

Blazars are the dominant extragalactic sources detected in the γ-ray sky by the *Fermi*-LAT [3]. These are a subclass of active galactic nuclei (AGNs) distinguished by their jets, which are directed towards our line of sight [4]. Blazars are notable for their intense γ-ray emissions, produced by relativistic jets. These jets, composed of nonthermal plasma, originate near supermassive black holes and extend over kpc/Mpc scales [5]. Blazars exhibit variability in both flux and spectrum across the electromagnetic spectrum, with timescales ranging from minutes to years [6,7]. Their high-energy emission and broadband variability (radio to γ ray) make them crucial targets for multiwavelength studies [8,9]. The continuous monitoring capabilities of *Fermi*-LAT in the 20 MeV to over 300 GeV range makes it an essential tool for investigating blazar variability in the high energy regime [1,10,11].

Blazars are commonly divided into two groups: BL Lac objects and flat spectrum radio quasars (FSRQs), primarily distinguished by their optical spectrum characteristics.

*Contact author: shahzahir4@gmail.com
†Contact author: darprince46@gmail.com

BL Lac objects exhibit weak or absent emission line features (EW < 5 Å), while FSRQs display prominent emission lines (EW > 5 Å) [4]. The broadband spectral energy distribution (SED) of blazars shows two humps, the first hump peaks in the optical/UV/x-ray energies, while the second hump peaks in the GeV energies. The low energy hump is well explained by the synchrotron emission from the relativistic electrons, while the high energy hump is mostly explained by the inverse Compton scattering [12–15]. Alternatively, high-energy emission can also arise from hadronic processes, where relativistic protons drive emission through proton-synchrotron radiation and pion production mechanisms [12,16].

Since the launch of the *Fermi* γ-ray telescope in 2008, the number of blazars that are known to be emitters of γ rays has drastically increased. The study of γ-ray variability in blazars has become a major focus in astrophysics. The long-term monitoring provided by the LAT has been essential for understanding the variability patterns of blazars, shedding light on the underlying physical processes at play. The continuous observations by the LAT have enabled extensive studies of blazar variability across multiple timescales, from minutes to years. This has been particularly valuable in multiwavelength campaigns that aim to study long-term correlated variability in AGN [17]. For instance, the detection of systematic lags between optical and γ-ray flares [18,19] and evidence of quasiperiodic variations in BL Lac objects [20] have provided critical insights into the physics of relativistic jets.

Despite extensive studies over the years, most blazar research has focused on individual sources using multiwavelength data [21–24]. However, few studies have examined the γ-ray flux variability characteristics of a large sample of blazars. Notable early work by [3] analyzed 11 months of *Fermi*-LAT data for 106 objects, and more recent research by [25] investigated the γ-ray flux variability of high-redshift ($z > 3$) blazars. Systematic studies of γ-ray variability in large blazar samples using *Fermi*-LAT data are crucial for advancing our understanding of these enigmatic sources. By focusing on γ-ray flux variability, we can uncover patterns and behaviors that are key to deciphering the physical processes driving blazar emissions.

The long-term dataset available for a large sample of blazars allows for comprehensive analyses to characterize their γ-ray variability. This study aims to characterize the long-term γ-ray variability of blazars on different timescales (three-day, seven-day, and 30-day). The characterization includes examining flux variability amplitude, flux distribution, index-flux relation, power spectral density (PSD), and spectral distribution. We utilize light curves from the *Fermi*-LAT Light Curve Repository (LCR), developed by Abdollahi *et al.* [26]. This public database provides light curves for various *Fermi*-LAT sources across different timescales, produced through likelihood analyses of the sources and their surroundings, yielding measurements of flux and spectral index. The paper is organized as follows: Section II gives the details of the sample of blazars; Sec. III discusses the temporal study of blazars, including spectral index distribution and flux-index correlation; Secs. IV and V cover the PSD and index distribution study, respectively; Sec. VI offers a summary and discussion; and finally, the conclusion is provided in Sec. VII.

II. SAMPLE OF BLAZARS

A. *Fermi*-LAT

The *Fermi*-LAT is a pair-conversion γ-ray telescope designed to detect photons with energies exceeding 20 MeV [1,27]. The LAT operates mainly in a scanning mode, surveying the entire sky every three hours [1]. It has a large effective area of around 8000 cm^2 for 1 GeV photons and has a broad field of view of approximately 2.4 steradians. This research focuses on extracting γ-ray data from the *Fermi*-LCR for all recorded blazars.

The LCR targets sources listed in the 4FGL-DR2 catalog with variability indices greater than 21.67 [28,29]. This catalog, based on a ten-year survey, indicates that sources with a variability index above 21.67 over 12 intervals have less than a 1% chance of remaining steady. Most of these variable sources are blazars, categorized as flat spectrum radio quasars (FSRQ), BL Lacertae objects (BL Lacs), and blazar candidates of unknown type (BCUs). The LCR provides three-day, seven-day, and 30-day binned light curves for each of these sources over more than 13 years of data involves analyzing. The LCR includes 794 sources as FSRQs, 1456 sources as BL Lacs, and 1493 sources as BCUs. The LCR analysis employs the standard *Fermi*-LAT science tool (version v11r5p3) and utilizes the *P8R2_SOURCE_V6* instrument response functions on *P8R3_SOURCE* class photons within an energy range of 100 MeV to 100 GeV. Light curves generated by the LCR are derived through unbinned likelihood analysis. The count distribution for each source of interest is modeled as a point source, incorporating all γ-ray sources from the 4FGL-DR2 catalog within a 30° radius of each region of interest. The normalization of each variable source in the region is allowed to vary, while the spectral parameters remain fixed to their catalog values. The model also includes Galactic and isotropic background components. The Galactic component *gll-iem-v07.fits* accounts for interstellar diffuse γ-ray emission from the Milky Way, and the isotropic component *iso_P8R3_SOURCE_V3_v1* accounts for residual charged-particle backgrounds and isotropic celestial γ-ray emission. Both Galactic and isotropic component normalizations are set free to vary during the fit.

To maximize the likelihood of the observed data given the model, the free parameters are adjusted. Initially, the normalization of the source spectrum varies freely, while spectral parameters are fixed to their 4FGL-DR2 catalog

values. After achieving a satisfactory fit, a second fitting round allows the photon index of the source of interest to vary. The likelihood analysis uses a test statistic, which is twice the ratio of the likelihood evaluated with background only to the likelihood evaluated including the source of interest. Using this test statistic as the detection criterion, the LCR estimates the observed LAT flux for sources with TS ≥ 4 and uses a Bayesian profile likelihood method to calculate upper limits for intervals yielding TS < 4. There are multiple ways to download the LCR data for off-line analysis. The light curve data for individual sources can be downloaded in CSV or JSON formats through their specific Source Report pages.

III. RESULTS

A. Temporal analysis

In this section, we present a detailed temporal analysis of the three-day, seven-day, and 30-day bin light curves of blazars acquired from the *Fermi*-LAT LCR, alongside flux values; we have also used the index values from the LCR. These light curves encompass an energy range of 0.1–100 GeV. We have focused on data points where TS > 4 (2σ detection) and flux/flux$_{\rm err} > 2$ to ensure the maximum data retention. After applying these criteria, the number of sources that remain in the (three-day, seven-day, and 30-day) bins are as follows: FSRQs (573, 572, 565), BL Lacs (456, 437, 389), and BCUs (335, 334, 302). The analysis in different time bins will help in understanding the effects of binning on the variability of the source, since almost every light curve we observe has some sort of binning associated. The large sample of light curves of blazars available in the three time bins offers a good platform for this kind of study. The variability amplitude is an important parameter that can be deduced from the light curves, which in turn can provide constraints on the physical processes that cause γ-ray flux variations. Therefore, we calculated the fractional variability amplitude ($F_{\rm var}$) as defined in [30] using the equation

$$F_{\rm var} = \sqrt{\frac{S^2 - \overline{\sigma_{\rm err}^2}}{\bar{F}^2}}, \tag{1}$$

where S^2 represents the variance of the fluxes, $\bar{F}$ is the mean flux, and $\overline{\sigma_{\rm err}^2}$ is the mean square error of the fluxes. The uncertainty on $F_{\rm var}$ is determined using the equation:

$$F_{\rm var,err} = \sqrt{\frac{1}{2N}\left(\frac{\overline{\sigma_{\rm err}^2}}{F_{\rm var}\bar{F}^2}\right)^2 + \frac{1}{N}\frac{\overline{\sigma_{\rm err}^2}}{\bar{F}^2}}, \tag{2}$$

where N is the number of points in the light curve. In Fig. 1, we show the histograms of the fractional variability for FSRQs, BL Lacs, and BCUs objects in the three time bins (three-day, seven-day, and 30-day). In the histograms, we have considered the blazars for which the $F_{\rm var}/F_{\rm var,error} > 2$. The mean fractional variability values for FSRQs, BL Lac, and BCU objects are given in Table I. Though there is no clear distinction between the histograms of FSRQs, BL Lacs, and BCUs in all of the time bins, however, the mean values of $F_{\rm var}$ reveal that FSRQ objects tend to exhibit higher variability compared to BL Lac across all three time bins. In three-day binned γ-ray light curves, BCUs' mean variability values are closer to those of FSRQ. However, in the seven-day and 30-day binned γ-ray light curves, the BCU mean variabilities are closer to the BL Lacs. These results imply that there are effects of binning on the $F_{\rm var}$ values. Further, to statistically test the differences, a two-sample Kolmogorov-Smirnov (KS) test was applied to the $F_{\rm var}$ values at the 95% confidence level. The comparison of the KS statistic between FSRQs, BL Lacs, and BCUs across different time bins is presented in Table I. These results demonstrate a statistically significant difference in variability distributions between FSRQs and BL Lacs, as well as between FSRQs and BCUs, particularly in the seven-day and 30-day time bins. However, the null hypothesis probability values rule out the differences between BL Lacs and BCUs. The KS test results between BL Lacs and BCUs suggest no significant variability differences, indicating that BL Lacs and BCUs may exhibit similar variability patterns in the observed time bins. This suggests that fractional variability is useful for distinguishing FSRQs from BL Lacs, but less effective in differentiating BL Lacs from BCUs. The higher variability observed in FSRQs could be linked to intrinsic physical processes, such as more active central engines or distinct jet structures compared to BL Lacs.

B. Effect of time binning on the $F_{\rm var}$

To further investigate the effect of binning on $F_{\rm var}$ values, we analyzed the $F_{\rm var}$ values for FSRQs, BL Lacs, and BCUs as a function of time binning intervals—specifically, three-day, seven-day, and 30-day bins. Only statistically significant flux points were included in the $F_{\rm var}$ calculation to ensure accurate results. In Table I, we have shown the weighted average values of the $F_{\rm var}$ for FSRQs, BL Lacs, and BCUs. The average $F_{\rm var}$ values clearly illustrate distinct variability behaviors among the blazar classes as a function of the time-binning interval; FSRQs exhibit a steady increase in $F_{\rm var}$ from 0.96 ± 0.001 at the three-day bin to 1.07 ± 0.001 at the 30-day bin, indicating that their variability amplitude is more pronounced on longer timescales, whereas BL Lacs show a modest rise from 0.64 ± 0.002 to 0.66 ± 0.002 between the three-day and seven-day bins, followed by a decrease to 0.62 ± 0.002 at the 30-day bin, suggesting a dominance of shorter-term variability; BCUs, on the other hand, maintain a relatively constant $F_{\rm var}$ (around 0.80 ± 0.004 to 0.81 ± 0.004) across all binning. The FSRQ variability pattern across time bins is consistent with previous study such as Akbar *et al.* [23];

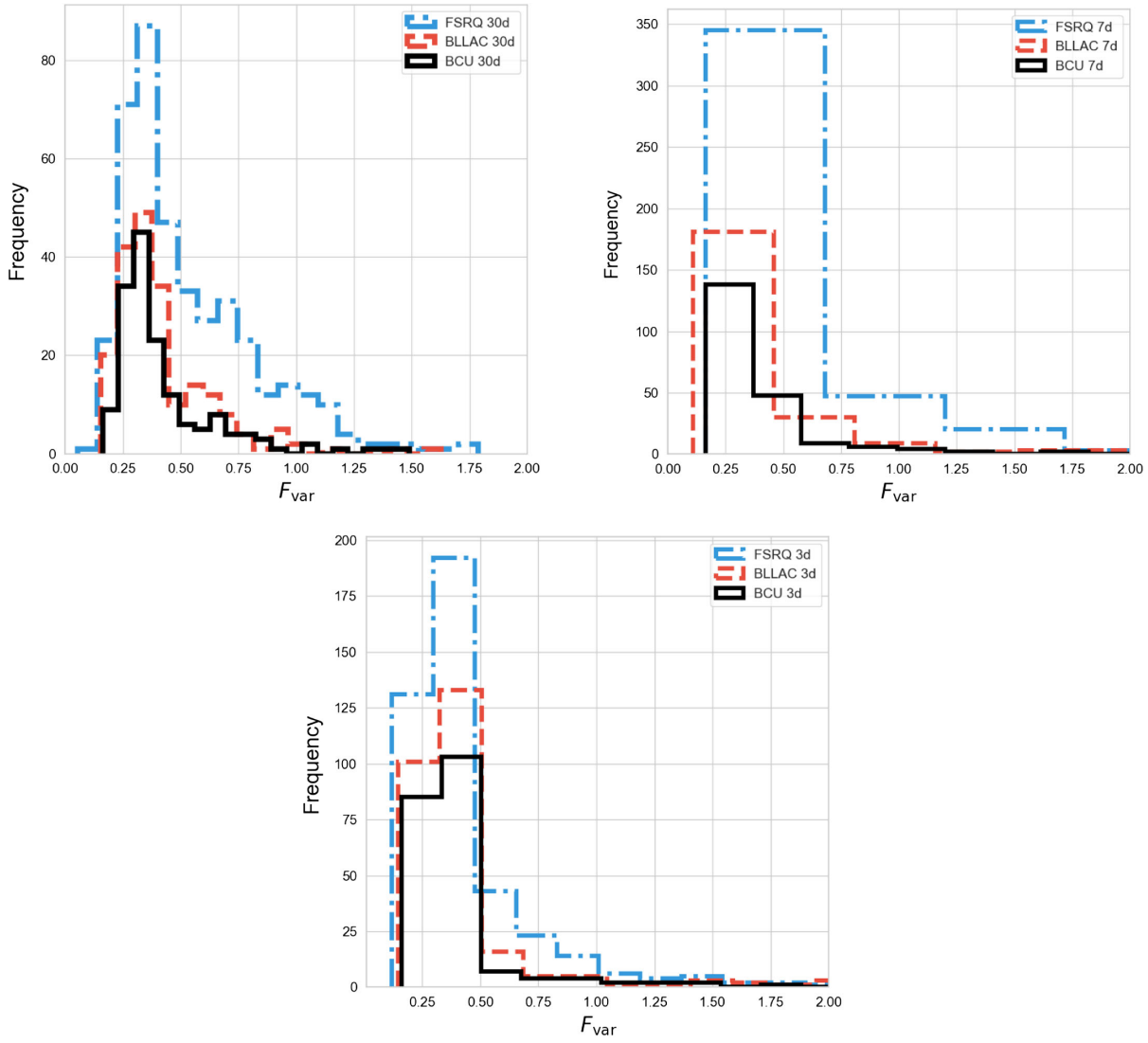

FIG. 1. Distribution of F_{var} for FSRQs, BL Lacs, and BCUs. The three panels represent histograms of light curves binned over three-day, seven-day, and 30-day intervals. The black solid histogram corresponds to BCUs, the red dashed histogram to BL Lacs, and the blue dash-dotted histogram to FSRQs. The results indicate that FSRQs generally exhibit higher variability compared to BL Lacs and BCUs.

TABLE I. The top part of the Table presents the weighted mean F_{var} values for FSRQs, BL Lacs, and BCUs, derived from light curves binned at three-day, seven-day, and 30-day intervals, with selection criteria of TS $>$ 4 and Flux/Flux$_{err}$ $>$ 2. The bottom part of the Table presents the KS test p values used to assess the statistical significance of differences in distributions between the FSRQs, BL Lacs, and BCUs for the light curves, based on the same binning intervals and selection thresholds as in the top part of the Table.

		F_{var}		
	Blazar type	Three-day	Seven-day	30-day
Mean F_{var}	FSRQs	0.96 ± 0.001	1.02 ± 0.001	1.07 ± 0.001
	BL Lacs	0.64 ± 0.002	0.66 ± 0.002	0.62 ± 0.002
	BCUs	0.80 ± 0.004	0.81 ± 0.004	0.81 ± 0.004
KS-statistic comparison		KS statistic (p value)		
		Three-day bin	Seven-day bin	30-day bin
	FSRQs vs BL Lacs	0.11 ($p = 0.03$)	0.16 ($p = 4.3 \times 10^{-4}$)	0.20 ($p = 1.85 \times 10^{-5}$)
	FSRQs vs BCUs	0.12 ($p = 0.01$)	0.21 ($p = 3.10 \times 10^{-6}$)	0.24 ($p = 9.94 \times 10^{-6}$)
	BL Lacs vs BCUs	0.08 ($p = 0.30$)	0.09 ($p = 0.19$)	0.08 ($p = 0.64$)

TABLE II. Summary of F_{var} values for the three brightest and three faintest FSRQs across three-day, seven-day, and 30-day binned light curves. The light curves contains time bins having TS > 4 and Flux/Flux$_{err}$ > 2. Each time-bin column includes subcolumns for the number of flux points, mean flux, and F_{var} values.

		Three-day			Seven-day			30-day		
FSRQ type	Source	Number	Mean flux	F_{var}	Number	Mean flux	F_{var}	Number	Mean flux	F_{var}
Bright FSRQ	4FGL 1427.9 − 4206	1491	6.57×10^{-7}	0.78 ± 0.004	706	6.08×10^{-7}	0.82 ± 0.005	180	5.65×10^{-7}	0.82 ± 0.004
	4FGL 1833.6 − 2103	1403	1.14×10^{-6}	1.45 ± 0.007	724	9.77×10^{-7}	1.50 ± 0.006	185	9.27×10^{-7}	1.50 ± 0.005
	4FGL 2253.9 + 1609	1633	1.40×10^{-6}	1.42 ± 0.002	752	1.30×10^{-6}	1.43 ± 0.002	184	1.33×10^{-6}	1.60 ± 0.002
Faint FSRQ	4FGL 2023.6 − 1139	10	2.43×10^{-7}	0.41 ± 0.18	9	1.33×10^{-7}	0.33 ± 0.25	7	4.46×10^{-8}	0.51 ± 0.28
	4FGL 2050.4 − 2627	17	1.63×10^{-7}	0.39 ± 0.16	12	1.14×10^{-7}	0.73 ± 0.15	10	3.85×10^{-8}	0.30 ± 0.17
	4FGL 1615.6 + 4712	8	1.00×10^{-7}	0.38 ± 0.22	8	6.84×10^{-8}	0.43 ± 0.20	5	2.01×10^{-8}	0.27 ± 0.33

the authors reported that F_{var} of FSRQ source PKS 0805-07 tends to increase with larger bin sizes when data points with $TS > 4$ are considered. In contrast, Schleicher *et al.* [31] work on the BL Lac source showed that the increase in bin size decreases the F_{var}. However, the authors considered all data points regardless of uncertainties. FSRQs are comparatively brighter than BL Lacs at γ-ray energy. To investigate the role of source brightness, we selected the three bright and three faint FSRQs and BL Lacs based on the mean flux values from the 30-day binned light curves. Tables II and III present the mean F_{var} values for these selected bright and faint FSRQs and BL Lac sources. For bright FSRQs, F_{var} exhibits an increasing trend with larger bin sizes, rising from three-day to 30-day intervals, while for bright BL Lac sources, F_{var} increases from three-day to seven-day bins but then declines as the bin size extends to 30 days. These results are consistent with the average behavior of these two classes. Additionally, the errors on F_{var} in bright sources remain small and largely independent of bin size. In contrast, for the faint FSRQs, the trend in F_{var} is less consistent and fluctuates without a clear trend. This is due to the reduction in the larger number of data points from the light curves and therefore is a direct manifestation of photon statistics bias. In either cases, the F_{var} values changing with the time suggests that we should maintain consistent time binning. This is critical when comparing variability across different energy bands to ensure reliable conclusions. In summary, these trends underscore two points: photon statistics bias strongly affects F_{var} in faint sources, and consistent time binning is critical when comparing variability across energy bands, to avoid misinterpreting bin size effects as intrinsic physical differences.

IV. FLUX-INDEX CORRELATION

The *Fermi* LCR provides the index information apart from the flux values discussed in the previous section. We considered the index and flux values where the ratio of index to its error and the ratio of flux to its error were greater than 2. We also excluded time periods with an index value exceeding 6 to remove outlier points. We used the Spearman rank correlation method to investigate the expected correlation between index and flux values for all of the sources in the three days, seven days, and 30 days binned light curves. This method gives us a rank coefficient and a probability value for the null hypothesis. In Fig. 2, we displayed the distribution of rank coefficients for the three types of blazars across three time periods. The results indicate that the spectral index and flux are positively correlated for most BL Lac and BCU sources across all time bins. Similarly, FSRQs exhibit a negative correlation between the index and flux, albeit with a reduced

TABLE III. Summary of F_{var} values for the three brightest and three faintest FSRQs across three-day, seven-day, and 30-day binned light curves. The light curves contain time bins having TS > 4 and Flux/Flux$_{err}$ > 2. Each time-bin column includes subcolumns for the number of flux points, mean flux, and F_{var} values.

		Three-day			Seven-day			30-day		
BL Lac type	Source	Number	Mean flux	F_{var}	Number	Mean flux	F_{var}	Number	Mean flux	F_{var}
Bright BL Lac	4FGL 2202.7 + 4216	1530	5.32×10^{-7}	0.93 ± 0.004	742	4.84×10^{-7}	0.95 ± 0.004	187	4.55×10^{-7}	0.90 ± 0.004
	4FGL 0721.9 + 7120	1498	2.17×10^{-7}	0.55 ± 0.006	754	1.94×10^{-7}	0.61 ± 0.006	187	1.86×10^{-7}	0.56 ± 0.006
	4FGL 1104.4 + 3812	1713	1.89×10^{-7}	0.38 ± 0.007	779	1.82×10^{-7}	0.40 ± 0.007	187	1.79×10^{-7}	0.37 ± 0.006
Faint BL Lac	4FGL 0051.2 − 6242	11	7.11×10^{-8}	0.24 ± 0.29	13	3.43×10^{-8}	0.18 ± 0.34	38	1.13×10^{-8}	0.24 ± 0.12
	4FGL 1150.6 + 4154	14	1.09×10^{-7}	0.09 ± 0.53	14	3.79×10^{-8}	0.46 ± 0.18	47	1.06×10^{-8}	0.18 ± 0.14
	4FGL 1610.7 − 664	11	2.87×10^{-7}	0.99 ± 0.19	8	1.23×10^{-7}	0.88 ± 0.29	38	1.11×10^{-8}	0.21 ± 0.16

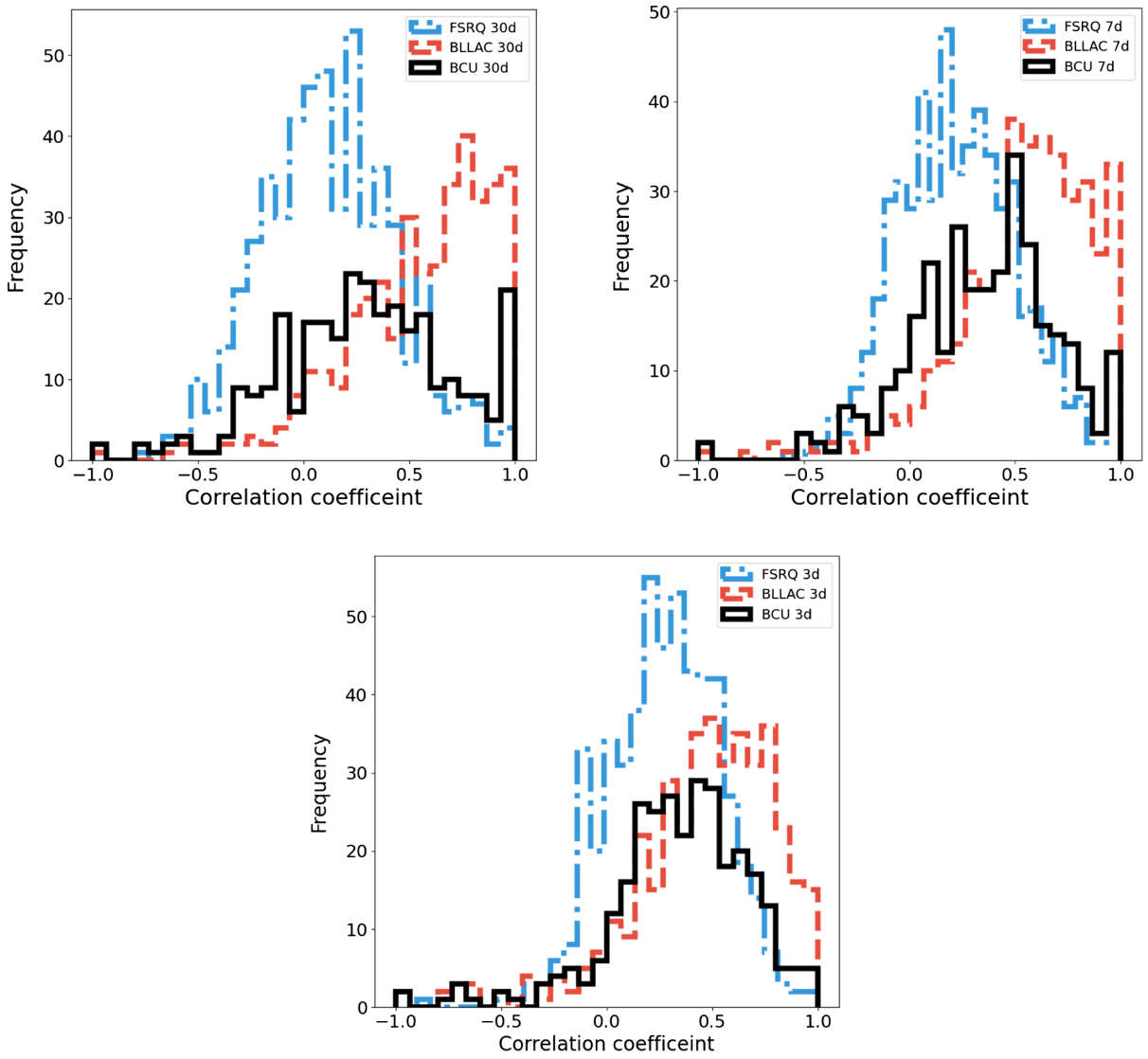

FIG. 2. Distribution of the correlation coefficient between flux and spectral index for FSRQs, BL Lacs, and BCUs using 30-day (top left), seven-day (top right), and three-day (bottom) binned light curves. Only time bins with TS > 4, $\mathrm{Flux}/\mathrm{Flux}_{\mathrm{err}} > 2$, and $Index/Index_{err} > 2$ are included. The results show a predominantly positive correlation for BL Lacs and BCUs, while FSRQs tend to exhibit negative correlations across all time bins.

correlation magnitude. To explore this further, we calculated the mean flux and mean index for each source. Figure 3 displays scatter plots of the mean index versus mean flux for FSRQ, BL Lac, and BCU sources across the time bins. The Spearman rank correlation analysis between the mean flux and mean spectral index for BL Lacs, FSRQs, and BCUs, across three-day, seven-day, and 30-day time bins, are presented in Table IV.[1] These values reveal distinct trends among FSRQS, BL Lacs, and BCUs. BL Lacs show a moderate positive correlation in all bins, with $r_s \approx 0.46$–0.47 and P values ($P_s \approx 10^{-22}$–10^{-23}), indicating that, as the flux increases, these sources become spectrally softer. If the spectral index becomes more negative, then the high-energy photons are fewer relative to lower energies. This can be explored under the physical scenario, where the acceleration process is more efficient, but the cooling is also stronger, leading to a balance where the electron distribution has a steeper slope. BCUs exhibit a similar mild positive correlation, with r_s values ranging from 0.25–0.36 and P values ($P_s \approx 10^{-6} - 10^{-10}$), implying a comparable trend of spectral softening with increasing flux. In contrast, FSRQs show a slight anticorrelation trend, with r_s values between -0.02 and -0.12, suggesting a marginal tendency for these sources to become spectrally

[1]While the Spearman rank correlation coefficient is below 0.5 in most cases, the corresponding low p values indicate that the trends, albeit weak, are statistically significant and not likely due to random fluctuations. This is a consequence of the large sample size, which increases the sensitivity of statistical tests.

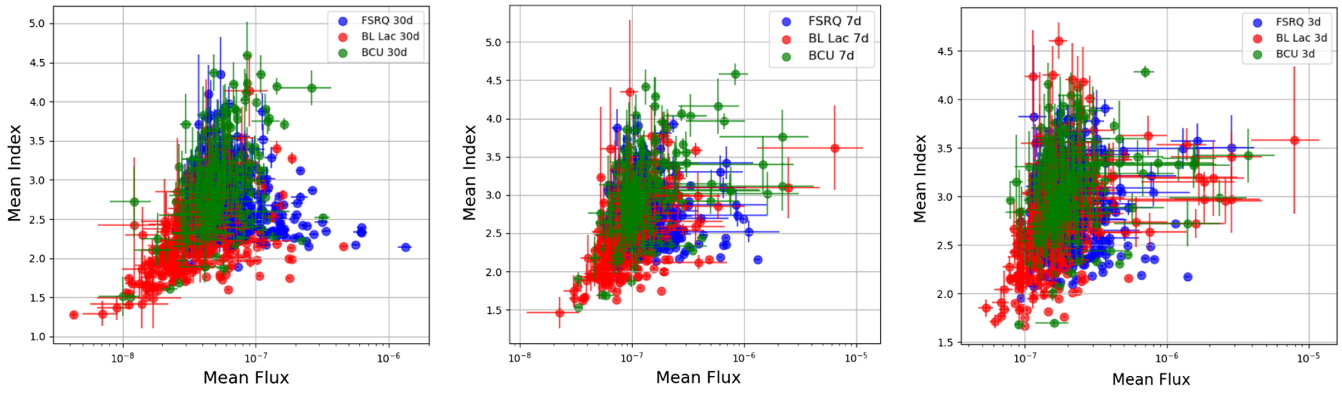

FIG. 3. Scatter plots showing the relationship between mean spectral index and mean flux for three time-binned light curves: 30-day (left), seven-day (middle), and three-day (right), for FSRQs, BL Lacs, and BCUs. The results suggest a mild positive correlation between index and flux for BL Lacs, and BCUs, whereas FSRQs exhibit an anticorrelation trend.

harder as flux increases. While P values for the seven-day and 30-day bins reject the null hypothesis that the index fluxes are not correlated, for the three-day bin light curve the null hypothesis cannot be rejected. The lack of correlation at the three-day bin indicates that short-term variability may obscure any consistent flux-index relationship in FSRQs. These results indicate that blazars exhibit complex and varied behavior depending on the type of blazar and the timescale of observation. This could reflect different physical mechanisms active over longer timescales, with changes in particle acceleration, cooling, or the surrounding environment influencing spectral properties. The cumulative behavior of blazars, integrating both flaring and quiescent states over extended periods, underscores the importance of multitimescale observations to fully understand the variability and emission processes in these sources.

A. Flux distribution

The examination of long-term flux distributions in the light curves of astrophysical systems is a valuable approach for understanding the physical processes driving variability. A normal flux distribution typically points to additive processes, whereas a log-normal distribution suggests the influence of multiplicative processes. In compact black hole systems, the flux distribution is generally observed to follow a log-normal pattern. To investigate this behavior in blazars, we analyzed the γ-ray flux distribution across three time bins (three-day, seven-day, and 30-day) using the Anderson-Darling (AD) test and histogram fitting. The AD test provides a test statistic (TS) value, and if the TS exceeds the critical value (CV) at a 5% significance level, the normality of the flux distribution is rejected.

We considered the flux points in the light curve where the fitting was convergent and included the points for which TS was greater than 4. Additionally, the flux/flux$_{\rm error} > 2$ was also included in the analysis to remove the flux points with large errors. Moreover, we removed the outlier points by choosing the flux values with values less than 10^{-9}. We used the Anderson-Darling (AD) test to confirm the log-normality of flux distributions in the blazar light curves. The number of sources showing log-normality is mentioned in Table V. For the sources which showed log-normal distribution, we fitted the normalized histograms in log scale with a Gaussian distribution, described by the equation

$$L(x) = \frac{1}{\sqrt{2\pi}\sigma} e^{-(x-\mu)^2/2\sigma^2}. \quad (3)$$

TABLE IV. Spearman rank correlation results (r_s and P_s) between mean flux and mean spectral index for BL Lacs, FSRQs, and BCUs across three-day, seven-day, and 30-day binned light curves. Column 1 lists the blazar type; Columns 2, 3, and 4 show results for three-day, seven-day, and 30-day bins, respectively, with each containing the correlation coefficient (r_s) and p value (P_s) as subcolumns.

	Three-day bin		Seven-day bin		30-day bin	
Blazar type	r_s	P_s	r_s	P_s	r_s	P_s
BL Lacs	0.46	3.98×10^{-22}	0.47	8.87×10^{-23}	0.47	4.33×10^{-23}
FSRQs	−0.02	0.69	−0.11	8.30×10^{-3}	−0.12	4.85×10^{-3}
BCUs	0.25	9.08×10^{-6}	0.34	1.53×10^{-9}	0.36	3.87×10^{-10}

TABLE V. Number of sources showing log-normality and the number of sources where log-normality was rejected for FSRQs, BL Lacs, and BCUs across three-day, seven-day, and 30-day binned light curves. Column 1 lists the blazar type; Columns 2 and 3 are meant for sources in which log-normality is accepted and rejected respective, with each containing subcolumns representing number of sources in the three day, seven day, and 30 day.

	LN accepted			LN rejected		
Blazar type	N_3	N_7	N_{30}	N_3	N_7	N_{30}
BL Lacs	326	326	335	130	111	54
FSRQs	311	314	395	262	258	170
BCUs	234	249	243	101	85	59

This equation fitted to normalized histogram in log-scale results in log-normal fit. Here μ and σ are the centroid and width of the logarithm of flux distribution. We analyzed the scatter plot between μ and σ, obtained from the log-normal fit (see Fig. 4). In the three-day binned light curves, no clear distinction is observed among BL Lac, FSRQ, and BCU sources. However, BL Lac sources exhibit a broader scatter compared to FSRQs and BCUs, which is consistent with the fact that BL Lacs encompass three subclasses: LBLs, IBLs, and HBLs. The Spearman rank correlation results (r_s and P_s values) across the three binned light curves are given in Table VI. The results suggest that, for BL Lacs, there is no correlation between μ and σ at the three-day bin, but a moderate positive correlation emerges at the seven-day bin, indicating some relationship between the parameters on this timescale, though it weakens again at the 30-day bin. In contrast, FSRQs show a progressively stronger positive correlation as the time bin increases, suggesting a greater relationship between μ and σ over longer timescales. BCUs, however, exhibit no significant correlation across any time bin, indicating that the centroid and width of the log-normal fit remain largely independent for this class of blazars. This variability behavior highlights distinct differences in how μ and σ relate across different blazar classes and timescales.

TABLE VI. Spearman rank correlation results (r_s and P_s values) between μ and σ values obtained from the log-normal fit for BL Lacs, FSRQs, and BCUs, based on three-day, seven-day, and 30-day binned light curves.

Correlation between μ and σ (log-normal fit)						
	Three-day bin		Seven-day bin		30-day bin	
Blazar type	r_s	P_s	r_s	P_s	r_s	P_s
BL Lacs	−0.06	0.29	0.23	2×10^{-4}	0.11	0.08
FSRQs	0.21	2×10^{-4}	0.34	2×10^{-9}	0.45	2×10^{-18}
BCUs	0.09	0.19	0.09	0.20	0.10	0.21

Out of the total sources considered in our analysis, the number of sources where log-normality is rejected is shown in Table V. We checked the flux distribution of these sources with the bimodel probability density function (PDF) defined by

$$D(x) = \frac{a}{\sqrt{2\pi}\sigma_1} e^{-(x-\mu_1)^2/2\sigma_1^2} + \frac{1-a}{\sqrt{2\pi}\sigma_2} e^{-(x-\mu_2)^2/2\sigma_2^2}, \quad (4)$$

where a is the mixing fraction that determines the relative contributions of the two components. We further examined the correlations among the fitting parameters of the double log-normal distributions. The Spearman rank correlation analysis between the double log-normal parameters (μ_1, μ_2, σ_1, σ_2) for BL Lacs, FSRQs, and BCUs—evaluated across three-day, seven-day, and 30-day light curves—is summarized in Table VII and reveals the following relationships. For FSRQs, μ_1 and μ_2 consistently show mild positive correlations across all time bins, with the maximum correlation at seven days ($r_s = 0.41$, $P_s = 4.37 \times 10^{-6}$), and μ_1 vs σ_1 as well as μ_2 vs σ_2 also exhibit positive correlations, particularly at shorter timescales. In BL Lacs, μ_1 and μ_2 exhibit a significant positive correlation in the three-day light curve ($r_s = 0.57$, $P_s = 2.6 \times 10^{-4}$), which weakens at longer timescales, while σ_1 and σ_2 show a significant negative correlation at 30 days ($r_s = -0.64$, $P_s = 4.9 \times 10^{-3}$). In BCUs, μ_1 and μ_2 show significant positively correlation at three days ($r_s = 0.65$,

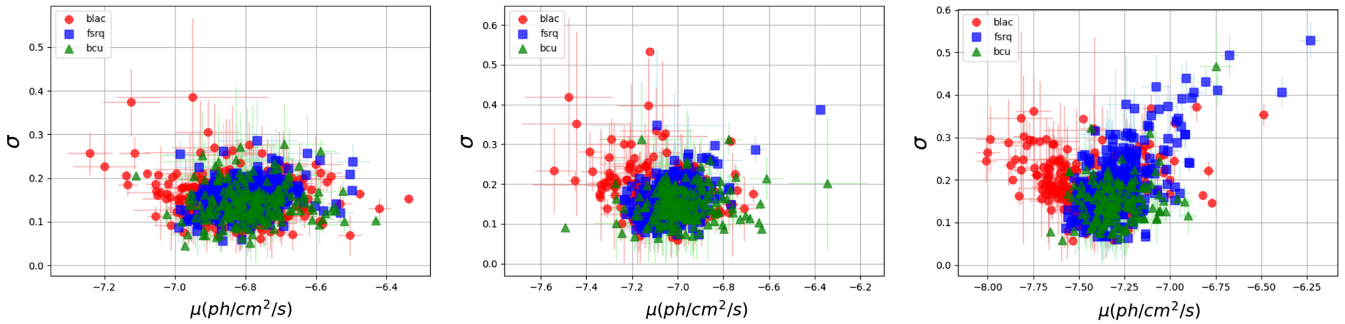

FIG. 4. Scatter plots of the log-normal fit parameters μ and σ for FSRQs, BL,Lacs, and BCUs, based on flux distributions from 30-day (left), seven-day (middle), and three-day (right) binned light curves. BL Lac sources exhibit greater scatter compared to FSRQs and BCUs.

TABLE VII. Spearman rank correlation results (r_s and P_s values) between the best fit parameters μ_1, μ_2, σ_1, and $\sigma 2$ obtained from the double log-normal fit for BL Lacs, FSRQs, and BCUs, based on three-day, seven-day, and 30-day binned light curves.

Blazar type parameters		r-value and p-value		
		Three-day	Seven-day	30-day
BL Lac	μ_1 vs μ_2	$0.57, 2.6 \times 10^{-4}$	0.27, 0.18	0.18, 0.48
	σ_1 vs σ_2	-7.7×10^{-4}, 0.99	−0.36, 0.07	$-0.64, 4.9 \times 10^{-3}$
	μ_1 vs σ_1	−0.03, 0.83	−0.06, 0.77	−0.04, 0.85
	μ_2 vs σ_2	0.25, 0.13	0.29, 0.15	0.05, 0.82
FSRQ	μ_1 vs μ_2	$0.36, 5.5 \times 10^{-5}$	$0.41, 4.37 \times 10^{-6}$	0.27, 0.02
	σ_1 vs σ_2	−0.18, 0.05	−0.01, 0.96	$-0.33, 3.2 \times 10^{-3}$
	μ_1 vs σ_1	$0.48, 2.59 \times 10^{-8}$	$0.50, 8 \times 10^{-9}$	$0.43, 1 \times 10^{-4}$
	μ_2 vs σ_2	$0.48, 3.43 \times 10^{-8}$	$0.43, 1.11 \times 10^{-6}$	0.03, 0.76
BCU	μ_1 vs μ_2	$0.65, 7.8 \times 10^{-4}$	0.47, 0.02	0.58, 0.04
	σ_1 vs σ_2	−0.02, 0.92	−0.09, 0.70	−0.35, 0.23
	μ_1 vs σ_1	0.34, 0.11	0.43, 0.04	−0.28, 0.35
	μ_2 vs σ_2	$-0.55, 5.9 \times 10^{-3}$	−0.04, 0.86	0.04, 0.88

$P_s = 7.8 \times 10^{-4}$), aligning with the trend observed in BL Lacs. However, μ_2 and σ_2 have a significant negative correlation at three days ($r_s = -0.55$, $P_s = 5.9 \times 10^{-3}$). These correlations suggest varying relationships between the log-normal parameters across different blazar classes and timescales, potentially reflecting different underlying physical mechanisms working at different timescales.

B. Effect of time binning on the flux distribution

The availability of light curves in the three time bins facilitated an examination of the effect of binning on the observed flux distributions. We analyzed the log-normality behavior of sources across three-day, seven-day, and 30-day binned light curves for BL Lacs, FSRQs, and BCUs. The analysis focuses on the number of sources exhibiting log-normality, including sources that are log-normal to a particular bin light curve or log-normal across multiple binned light curves. Our results show significant overlap in the log-normality distributions between different time binned light curves, although some sources demonstrate unique behavior depending on the binning interval. Table VIII provides a comprehensive summary of the total number of sources in each bin, along with the common and unique sources observed between pairs of time bins. The log-normality of blazar sources across different time bins reveals that, while a significant number of sources exhibit consistent log-normality in multiple time bins, the 30-day bin tends to introduce more unique sources, especially in FSRQs. This suggests that longer timescale observations capture different variability patterns than shorter ones, which could be attributed to different underlying physical processes. Interestingly, Shah *et al.* [32] demonstrated that, when a light curve contains a sufficiently large number of data points, binning does not significantly affect the log-normal nature of the flux distribution–provided the power spectral density (PSD) has a nonzero spectral slope. To test this, we examined the number of sources exhibiting log-normality in light curves binned over three, seven, or 30 days. Our focus was particularly on sources that are uniquely log-normal in one specific binning scheme and contain more than 300

TABLE VIII. Total sources, common, and unique sources showing log-normality across different binned light curves for BL Lacs, FSRQs, and BCUs. The first column shows the blazar type, the second column shows the total number of sources in each time bin (three-day, seven-day, 30-day) for BL Lacs, FSRQs, and BCUs. The rest of the columns show the common and unique sources between each combination of time bins (three-day and seven-day, three-day and 30-day, seven-day and 30-day). Unique sources are listed in parentheses, showing how many are unique to each bin.

		Three-day and seven-day		Three-day and 30-day		Seven-day and 30-day	
Blazar type	Total (three-day, seven-day, 30-day)	Common	Unique (three-day, seven-day)	Common	Unique (three-day, 30-day)	Common	Unique (seven-day, 30-day)
BL Lacs	326, 326, 330	244	(82, 80)	238	(88, 97)	250	(74, 85)
FSRQs	311, 314, 395	230	(81, 84)	235	(76, 160)	250	(64, 145)
BCUs	234, 249, 243	192	(42, 57)	173	(61, 70)	192	(57, 51)

significant data points. This analysis serves to verify the consistency between simulated light curve results reported by Shah *et al.* [32] and our observational findings. Further details are provided in the next section.

V. PSD

We analyzed the PSD of the γ-ray light curve, which exhibits log-normal flux distributions. To enhance statistical reliability, we focused on sources with more than 300 data points after implementing the quality cuts outlined earlier. More data points allowed the PSD to capture accurate details in the frequency domain. After applying the cuts, we identified 14 and ten sources in BL Lacs and FSRQs, respectively, possessing log-normality in the three-day binned γ-light curve, and 18 and eight sources in BL Lacs and FSRQs respectively, possessing log-normality in the seven-day binned γ-light curve, respectively. However, no BCU sources met the threshold, and no BL Lac or FSRQ sources qualified for the 30-day binned light curve. The PSDs are obtained using the Bartlett's method, splitting the light curve into equal-length segments, calculating the periodogram in each, and then averaging them into the final periodogram. We fitted the power law model to all averaged PSDs, the higher frequency were limited to 0.01 1/day, the fit parameters for the PSDs of the sources are summarized in Table IX. In all the PSDs, we noted no evidence of a break. The average power-law (PL) slope obtained in BL Lac and FSRQs are obtained as 0.43 ± 0.07 and 0.54 ± 0.10, respectively in three-day binned light curves, while 0.52 ± 0.09 and 0.85 ± 0.09 in seven-day binned light curves. A power law PSD suggests that there is no single characteristic timescale that dominates the behavior—instead, fluctuations occur over a wide, continuous range of timescales. This is a common signature of turbulent processes and shock-induced emission. The rebinning of lightcurves from three-day to seven-day bins, effectively averages out the short-timescale (high-frequency) variations. As a result, the relative power from longer timescales (low frequencies) becomes more prominent. A steeper power-law index indicates that low-frequency (longer timescale) fluctuations contribute more to the total variance than high-frequency ones.

For BL Lac sources showing log-normal behavior, we observed that the PSD index is less than 1 in 3 days. Notably, three sources—4FGL 0449.4-4350, 4FGL $1104.4 + 3812$, and 4FGL $1653.8 + 3945$—are log-normal in the three-day binned light curve but do not show single log-normal behavior in the seven-day binned light curve. The PSD of these three sources shows spectral slopes of 0.71 ± 0.08, 0.69 ± 0.07, and 0.26 ± 0.09, respectively. The seven-day binned light curve rejects the log-normality of these three sources and instead their flux distributions are better fitted with a double log-normal PDF, yielding reduced χ^2 values of 0.47, 1.05, and 0.50. These results indicate that log-normality though bimodel is still consistent within these sources. In the seven-day binned light curve, seven sources, namely, 4FGL $1555.7+1111$, 4FGL $1427.0 + 2348$, 4FGL $1217.9 + 3007$, 4FGL $1015.0 + 4926$, 4FGL $0538.8 - 4405$, 4FGL $0211.2 + 1051$, and 4FGL $1248.3 + 5820$, exhibit log-normal behavior, which is not observed in the three-day binned light curves. The PSD slopes of these sources have a wide spread from 0.15–1.40 with 4FGL $0538.8 - 4405$ showing a steep slope, which has PSD slopes of 1.40 ± 0.15. The flux distribution in the three-day binned light curves for these sources is better fitted by a double log-normal PDF.

Among the 11 BL Lacs showing log-normality in both the three-day and seven-day light curves, we found that the PSD slope of eight BL Lacs is less than 0.5, with a few consistent with white noise light curves. For these sources, the transition from three-day to seven-day binning does not alter the log-normality. This result is consistent with Shah *et al.* [33], which showed that the effect of binning becomes significant when averaging the data $\sim$8 times the baseline time interval, allowing log-normality to be rejected at the 10% significance level, and completely rejected if we average the data 64 times the baseline time interval. For FSRQs, among the ten sources showing log-normality in the three-day binned light curves, only 4FGL $2236.3 + 2828$ remains log-normal in the seven-day binned light curve. The sources that are not log-normal in the seven-day binned light curve exhibit double log-normality. Similarly, there are four FSRQs that show log-normality in the seven-day binned light curve but not in the three-day binned light curve; their distribution in the three-day binned light curve is double log-normal. It should be noted that there can be a number of effects that can, potentially, distort the PSD of our analysis from the "true" long-term variability pattern. This includes stochastic variability within a finite length of observation, systematic in the data, and statistical noise.

VI. SPECTRAL INDEX DISTRIBUTION

Given the narrow spread of the photon index distribution for each blazar type, significant changes in the photon index over time are not expected for a given source. Even though flux variations are substantial (by a factor of more than 7) in blazars, the photon index range is only about $\sim$0.3 wide, accounting for a 1σ dispersion. We analyzed the spectral index distribution for blazars exhibiting log-normal flux distributions, selecting sources with more than 100 data points in their light curves. Importantly, we found that the corresponding index distributions deviate from a Gaussian distribution, instead exhibiting either log-normal or double log-normal behavior. Our results indicate that the index values of FSRQ sources mostly follow a double log-normal distribution (see Table X). Specifically, in the three-day binning interval, 125 FSRQ sources exhibit a log-normal index distribution, while 147 show a double log-normal distribution. This trend is less pronounced in the seven-day binned light curves, where 72 sources show a

TABLE IX. PSD analysis results of the three-day and seven-day binned γ-ray light curves, each with more than 300 data points and showing log-normal flux distributions in either the three-day binning, the seven-day binning, or both. The upper half of the Table lists results for BL Lac sources, while the lower half corresponds to FSRQ sources. The left-side columns present the results for the three-day binning, and the right-side columns for the seven-day binning. Column 1, source name; columns 2–4, normalization, slope, and reduced χ^2 from the PL fit for the three-day binning light curves; columns 5–7, corresponding parameters for the seven-day binning.

	BL Lac (three-day bin)			BL Lac (seven-day bin)		
Source	Norm	Alpha	χ^2/dof	Norm	Alpha	χ^2/dof
4FGL 1517.7 − 2422	1.94 ± 0.29	0.53 ± 0.10	1.14	4.02 ± 0.49	0.40 ± 0.19	1.82
4FGL 1543.0 + 6130	2.95 ± 0.55	0.15 ± 0.13	2.27	2.20 ± 0.38	0.14 ± 0.26	1.06
4FGL 0222.6 + 4302	3.95 ± 0.66	0.72 ± 0.11	2.1	4.34 ± 0.45	0.91 ± 0.13	3.22
4FGL 0112.1 + 2245	1.61 ± 0.27	0.44 ± 0.12	1.94	5.09 ± 0.60	0.93 ± 0.19	1.69
4FGL 0449.4 − 4350	3.31 ± 0.39	0.71 ± 0.08	1.29			
4FGL 1104.4 + 3812	1.71 ± 0.18	0.69 ± 0.07	1.22			
4FGL 2000.0 + 6508	1.21 ± 0.25	0.49 ± 0.14	1.23	2.07 ± 0.29	0.32 ± 0.25	1.60
4FGL 1058.4 + 0133	2.50 ± 0.72	0.69 ± 0.20	1.41	5.11 ± 0.80	0.80 ± 0.25	2.60
4FGL 2139.4 − 4235	2.28 ± 0.34	0.27 ± 0.10	0.84	3.08 ± 0.57	0.32 ± 0.28	1.19
4FGL 1653.8 + 3945	0.81 ± 0.12	0.26 ± 0.09	1.44			
4FGL 2158.8 − 3013	3.31 ± 0.37	0.83 ± 0.07	0.93	4.83 ± 0.45	0.98 ± 0.12	1.27
4FGL 0144.6 + 2705	1.25 ± 0.18	0.10 ± 0.09	1.31	2.16 ± 0.31	0.02 ± 0.22	6.47
4FGL 0818.2 + 4222	1.88 ± 0.28	0.11 ± 0.13	0.65	1.76 ± 0.23	0.04 ± 0.17	0.46
4FGL 1806.8 + 6949	1.13 ± 0.21	0.10 ± 0.13	0.83	1.81 ± 0.27	0.32 ± 0.21	0.89
4FGL 1555.7 + 1111				2.92 ± 0.28	0.62 ± 0.15	1.52
4FGL 1427.0 + 2348				2.54 ± 0.27	0.22 ± 0.16	0.97
4FGL 1217.9 + 3007				3.46 ± 0.41	0.15 ± 0.18	1.11
4FGL 1015.0 + 4926				2.82 ± 0.32	0.52 ± 0.20	2.00
4FGL 0538.8 − 4405				3.22 ± 0.32	1.40 ± 0.15	3.72
4FGL 0211.2 + 1051				3.02 ± 0.48	0.43 ± 0.26	0.57
4FGL 1248.3 + 5820				3.47 ± 0.54	0.86 ± 0.26	4.71
	FSRQ (three-day bin)			FSRQ (seven-day bin)		
4FGL 0532.6 + 0732	4.73 ± 0.75	0.84 ± 0.11	0.43			
4FGL 1127.0 − 1857	2.06 ± 0.50	0.67 ± 0.16	1.39			
4FGL 0526.2 − 4830	1.94 ± 0.44	0.54 ± 0.15	1.47			
4FGL 0217.8 + 0144	1.40 ± 0.23	0.06 ± 0.12	0.86			
4FGL 0457.0 − 2324	3.04 ± 0.33	0.93 ± 0.07	1.23			
4FGL 1246.7 − 2548	3.93 ± 0.59	0.53 ± 0.09	0.87			
4FGL 0453.1 − 2806	2.33 ± 0.40	0.10 ± 0.11	1.04			
4FGL 2236.3 + 2828	1.94 ± 0.45	0.14 ± 0.15	1.80	5.85 ± 1.03	0.95 ± 0.29	1.27
4FGL 2345.2 − 1555	6.28 ± 1.53	1.01 ± 0.15	1.29			
4FGL 0407.0 − 3826	2.68 ± 0.43	0.58 ± 0.11	2.21			
4FGL 2348.0 − 1630				10.38 ± 1.59	0.90 ± 0.15	1.06
4FGL 2229.7 − 0832				6.70 ± 1.25	0.70 ± 0.18	1.84
4FGL 2356.4 + 4030				5.83 ± 0.83	0.56 ± 0.11	0.57
4FGL 1057.8 + 0138				4.99 ± 1.02	0.65 ± 0.14	0.63
4FGL 0909.1 + 0121				6.62 ± 1.38	0.77 ± 0.16	0.80
4FGL 1345.5 + 4453				8.16 ± 0.88	1.45 ± 0.10	1.79
4FGL 1256.1 − 0547				20.02 ± 1.86	0.80 ± 0.08	3.76

log-normal index distribution and 104 show a double log-normal distribution. However, BL Lac and BCU sources show a mixed trend in the three time bins (three-day, seven-day, and 30-day).

In addition to this, we also plotted the scatter between the μ and σ values obtained from the log-normal fit to the index distribution for the FSRQs, BL Lacs and BCUs across the three time bins (three-day, seven-day, and 30-day) in Fig. 5. The scatter plot in case of BL Lacs shows broader range values of centroid and sigma values compared to the FSRQs and BCUs. This is expected as BL Lac sources are composed of HBL, IBL, and LBL sources. This observation aligns with our findings from the flux distribution. Additionally, we examined the scatter between the μ_1 and σ_1 values, as well as the μ_2 and σ_2 values derived from the double log-normal fit for the index distributions of FSRQs, BL Lacs, and BCUs across the three time bins (see Fig. 6). While the plots show a slight difference in scatter

TABLE X. Summary of sources showing log-normal and double log-normal index distributions across different binning intervals.

Source type	Binning interval	Log-normal (No. of sources)	Double log-normal (No. of sources)
FSRQ	Three-day	125	147
	Seven-day	72	104
	30-day	23	67
BL Lac	Three-day	135	123
	Seven-day	78	101
	30-day	72	66
BCU	Three-day	82	75
	Seven-day	19	32
	30-day	4	4

between FSRQs and BL Lacs, there is no definitive evidence indicating whether BCUs are more aligned with FSRQs or BL Lacs.

These findings suggest that the variability in spectral index distributions is not random but instead follows distinct patterns in FSRQs, BL Lacs and BCUs. The dominance of double log-normal distributions, especially in FSRQs, points to a more complex variability mechanism at γ-ray energies compared to the simpler log-normal distributions observed in flux. This result diverges from previous studies of blazar behavior at x-ray energies [34], where the index distribution was found to be Gaussian while the flux distribution followed a log-normal pattern. The Gaussian index distribution at x-ray energies implies that perturbations in the acceleration timescale follow a Gaussian process, which in turn leads to the observed log-normal flux distribution. In contrast, the observation of log-normal index distributions at γ-ray energies suggests that flux variations in these sources are not directly tied to variations in the spectral index, indicating potentially different emission mechanisms or variability processes at higher energies.

VII. SUMMARY AND DISCUSSION

In this study, we carried a systematic analysis of long-term γ-ray data from the *Fermi*-LAT for blazars comprising FSRQs, BL Lacs, and BCUs to characterize their γ-ray

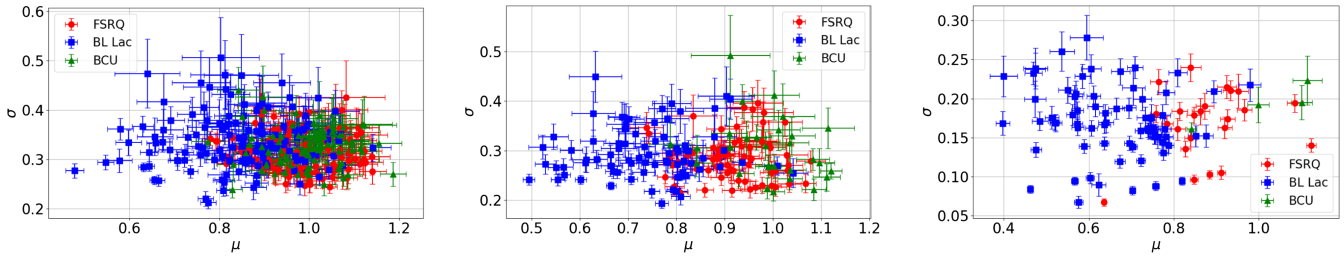

FIG. 5. The scatter plot shows the best-fit values of μ and σ obtained from log-normal fits to the spectral index distributions for the three blazar classes (BL Lacs, BCUs, and FSRQs) across three time binnings: three-day (left), seven-day (middle), and 30-day (right).

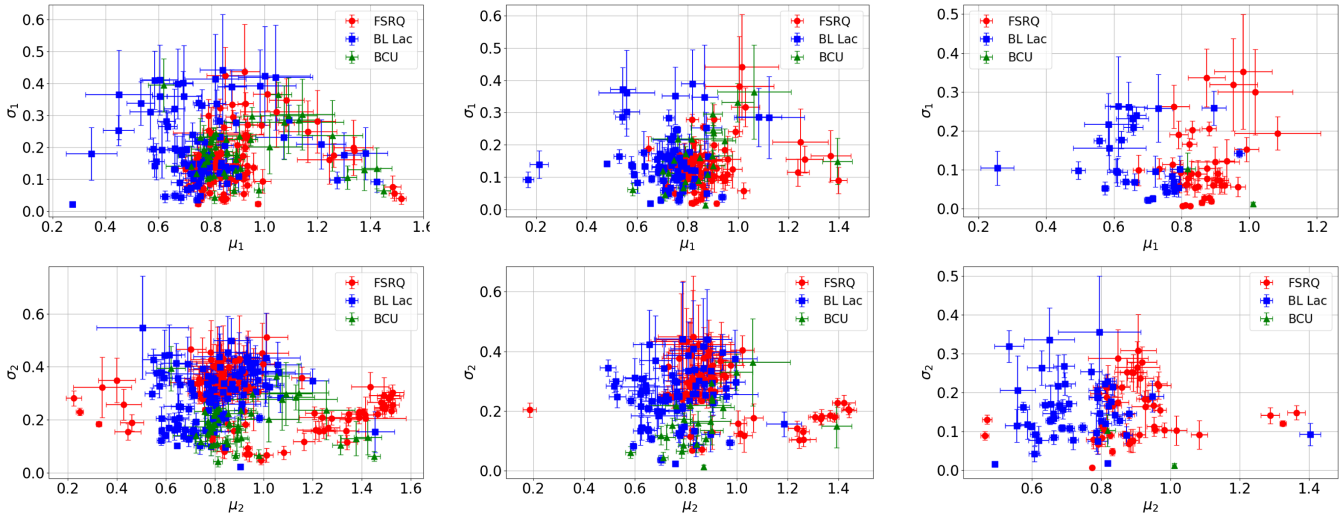

FIG. 6. The scatter plot between the μ_1 and σ_1 values (top panel), and μ_2 and σ_2 values (bottom panel) derived from the double log-normal fit for the index distributions of FSRQs, BL Lacs, and BCUs across the three time bins: three-day (left), seven-day (middle), and 30-day (right).

variability. We focused on three-day, seven-day, and 30-day binned light curves to assess how binning impacts variability. Using data where TS > 4 (a 2σ detection threshold), we examined F_{var} by constructing histograms of F_{var} across time bins. The results show that FSRQs exhibit higher mean variability compared to BL Lacs and BCUs, while BCUs demonstrate intermediate variability. A KS test reveals differences between FSRQs and BL Lacs, and between FSRQs and BCUs, particularly in seven-day and 30-day bins, while differences between BL Lacs and BCUs are not significant. These findings suggest that F_{var} may distinguish FSRQs from BL Lacs, but less so for BL Lacs versus BCUs. Similar variability between BL Lacs and BCUs implies that these sources share more common features, making it challenging to distinguish them solely based on variability metrics. These findings align with earlier studies [11,35] that indicate FSRQs tend to exhibit more pronounced variability due to more powerful jets and accretion processes. It is known that FSRQs occupy denser and more gas-rich environments than BL Lac objects, which in turn results in higher luminosity and variability. For example, Paggi *et al.* [36] noted that FSRQs feature the strong broad emission lines, clear evidence of abundant circumnuclear gas unlike in BL Lacs. On average, FSRQs are much more luminous than BL Lacs. In γ rays, for example, Rajput *et al.* [37] show that FSRQs cluster at much higher luminosities than BL Lacs by using the sample of *Fermi* blazars. The greater luminosity of FSRQs is also evident in emission lines: strong broad lines and dusty torus emission in FSRQs indicate more accretion power and richer photon fields, e.g., [38]. By contrast, BL Lacs often show only weak or no lines, consistent with low accretion luminosity. Therefore, the observation that a substantial fraction of BCUs exhibit variability characteristics closely resembling those of BL Lacs suggests that many BCUs may also inhabit similarly low-density environments.

In our study, we considered full light curves including the flaring and low flux states. We know a large fraction of blazars exhibit variability dominated by occasional strong flares separated by prolonged quiescent states. The variance statistic captures the total variability in the light curve, meaning that a few intense flares can contribute significantly to the overall variance. To examine this, one could analyze the light curves by separating flaring and quiescent states or use additional measures such as the fraction of total variance contributed by the highest flux states. In our analysis, the variability statistic does not explicitly distinguish between variability from frequent moderate fluctuations and variability dominated by rare, intense flares. However, one way to address this would be to compute the variance separately for different flux levels or analyze the light curves.

The analysis of the correlation between γ-ray flux and spectral index in blazars reveals a moderate positive correlation across different time binnings (three-day, seven-day, and 30-day) for BL Lacs and BCUs, indicating that they tend to become spectrally softer as their flux increases. This "softer when brighter" behavior contrasts with the commonly observed "harder when brighter" trend seen during short flaring events, where higher fluxes are typically associated with harder spectra [11,39]. Here, more particles may be injected with a harder spectrum (if acceleration is efficient), which would make the spectrum harder. But if the cooling is more efficient, the high-energy particles lose energy quickly, leading to a softer spectrum. So a rapid injection of particles and then quickly cooling lead to a steeper spectrum. This softer when brighter trend also suggests that the underlying physical processes governing long-term γ-ray emission in BL Lacs may involve shifts in particle acceleration or cooling mechanisms over time. In contrast, FSRQs exhibit a mild anticorrelation (see Table IV), suggesting a tendency for these sources to become spectrally harder as their flux increases. Statistical analysis shows that the p values for the seven-day and 30-day bins reject the null hypothesis of no correlation between flux and index, whereas for the three-day bin, the null hypothesis cannot be rejected. The absence of correlation in the three-day bin suggests that short-term variability may obscure any consistent flux-index relationship in FSRQs. This timescale dependence highlights a critical distinction: long-term trends reflect persistent physical mechanisms (e.g., sustained particle injection or gradual cooling), whereas short-term variability may arise from localized, transient phenomena like shocks or magnetic reconnection [40]. These findings imply that the environment near the blazar's central engine evolves over longer periods, influenced by factors such as magnetic field strength, particle density, and energy dissipation rates, which shape the spectral characteristics of the emission. The need for multitimescale observations becomes evident, as studies focusing solely on short-term variability may overlook the broader trends governing blazar behavior over time. These results highlight the importance of integrating data across different timescales to achieve a comprehensive understanding of these objects, as emphasized in previous works [41,42].

Our statistical study of both variance and index/flux correlation shows that a large fraction of BCUs eventually gets classified as BL Lacs. This aligns with previous studies that have found BCUs to exhibit similar nonthermal emission characteristics and variability amplitudes as BL Lacs [43–45]. In Fig. 3, where the mean index is plotted against mean flux, BL Lac sources tend to show larger scatter than FSRQs. This is expected, since BL Lac sources are composed of three subclasses, HBL, IBL and LBLs. Importantly, the results of variability analysis, which shows that BCUs are more likely to be BL Lac, are consistent with the flux vs index plot (Fig. 3) as both BL Lac and BCU show a mild brighter softer trend while FSRQs show a

slightly harder brighter trend. The narrow spread of BCUs suggests that the majority of them may belong to one subclass of BL Lacs. These results are consistent with [45] which used flare light-curve patterns and neural networks on 3FGL data and assign the majority of BCUs to BL Lac class. Studies such as Lefaucheur and Pita [46] applied machine-learning classifiers to *Fermi* BCUs: they found that ∼91% of their BCU sample were classified as BL Lac-like while only ∼3% were FSRQ-like. The authors of [43] in their optical spectroscopic observations of 37 sources, mostly BCUs, confirmed the BL Lac nature of 27 sources. This finding supports the idea that a significant fraction of BCUs are intrinsically BL Lacs.

The examination of long-term flux distributions in blazars provides key insights into the physical processes driving their variability. It is well established that purely additive fluctuations, arising from the linear sum of numerous independent, small-amplitude variations, lead to normally distributed total fluxes, as expected from the central limit theorem [30,47]. However, observational evidence across various accreting systems consistently reveals log-normal flux distributions, implying that the underlying variability mechanism is multiplicative in nature [48,49]. In accretion-powered sources like x-ray binaries and AGNs, this behavior is well explained by the "propagating fluctuations" model, where local variations in the mass accretion rate generated at different disk radii propagate inward, coupling multiplicatively and modulating the emission from the inner regions [48]. Interestingly, log-normality is also observed in non-thermal jet-dominated systems such as blazars [32–34], possibly due to the imprint of disk fluctuations onto the jet via efficient variability transmission mechanisms [50–52]. Nevertheless, observations of extremely rapid, high-energy variability suggest that jet emission can at times evolve independently of the disk [53–55]. In such scenarios, log-normal behavior may arise from intrinsic jet processes, such as linear Gaussian perturbations to particle acceleration or escape timescales [56], or even from additive processes like shot noise when modified by Doppler boosting from a population of randomly oriented minijets [57].

In our analysis, γ-ray flux distributions for blazars were studied across different time bins (three-day, seven-day, and 30-day) using the AD test. The AD test results confirmed log-normality in a significant number of BL Lacs, FSRQs, and BCUs, indicating that these systems exhibit multiplicative variability processes. Flux points with large errors were excluded to maintain data reliability, and outliers were filtered to focus on the general behavior of the systems. The absence of strong correlations between the μ and σ of the flux distribution across different time bins suggests that flux variations are driven by complex processes that do not depend solely on the average flux values. In the 30-day binned light curves, BCUs show a tendency to behave similarly to FSRQs, implying that longer observation periods may reveal patterns in their variability.

For sources where the log-normality of flux distributions was rejected, a bimodal PDF was fitted, indicating that some blazars may experience two distinct states of variability. Positive correlations between the centroids of the bimodal distributions in all blazars suggest that, when flux increases in one state, it tends to rise in the other as well, reflecting possible transitions between different physical states of activity. In contrast, the negative correlation between the widths of the distributions (σ_1 and σ_2), particularly for BL Lacs, points to variability behaviors, where the spread in flux decreases as the system enters a different state. Additionally, the analysis shows that FSRQs exhibit consistent positive correlations across multiple parameters, implying more structured variability. The results indicate that blazars, particularly BCUs, behave differently depending on the timescale of observation, with longer bins showing stronger correlations and clearer patterns of variability. In this study, many blazars retain log-normal behavior in both three-day and seven-day binned light curves, indicating that the multiplicative processes responsible for this behavior are persistent across these timescales. However, some sources only show log-normality in one binning scheme, which might indicate a transition between different variability modes. The observation of double log-normal flux distributions in some sources suggests that there could be two distinct multiplicative processes influencing the variability.

The PSD is calculated to study the variability patterns in blazars. Typically, the slope of the PSD provides insights into the nature of variability. A PSD slope close to 0 indicates white noise (random variability), while steeper slopes suggest more structured, long-term variability. The PSD slopes for BL Lacs are typically less than 1 in both three-day binned light curves. The PSD slopes in FSRQs tend to be steeper than those in BL Lacs, especially in the seven-day binned light curves. This suggests that the variability in FSRQs is not dominated by white noise but follows a more structured, red noise pattern (with longer timescales contributing more to variability). Notably, BL Lacs with PSD slopes consistent with white noise (e.g., 4FGL 1806.8 + 6949, slope 0.10 ± 0.13) may represent systems where short-timescale variability dominates, masking underlying trends. In our study, PSD slopes for BL Lac objects range from 0.1 to 0.83 for three-day binned light curves and from 0.02 to 1.40 for seven-day bins. For FSRQs, the PSD slopes range from 0.10 to 0.93 (three-day bins) and 0.56 to 1.45 (seven-day bins). These values are generally flatter than those reported in early studies such as Abdo *et al.* [58], who analyzed 11 months of seven-day binned light curves for bright blazars and found most PSD slopes in the range 1.1 to 1.6. Similarly, [59] reported R-band optical PSD slopes ranging from 0.6 to 2.3, with an average slope of -1.6 ± 0.3 across six blazars. However, they also noted significant variation between optical and γ-ray PSDs—for example, PKS

2155–304 showed a steep optical PSD (~ -2.2) but a much flatter γ-ray PSD [58], highlighting wavelength-dependent variability behavior. More recent studies, however, have reported flatter γ-ray PSD slopes consistent with our findings. Sobolewska *et al.* [60] examined four-year *Fermi*-LAT light curves of 13 bright blazars and found slopes typically ≤ 1, with no systematic difference between FSRQs and BL Lacs. Nakagawa and Mori [61] reported a slope of 0.38 ± 0.21 for Mrk 421, which is even flatter than the 0.69 ± 0.07 we obtained for the same source. Kushwaha *et al.* [62] analyzed seven-year *Fermi*-LAT data for Mrk 421, B2 $1520+31$, and PKS 1510–089, and their results for PKS 1510–089 agree with those from Tarnopolski *et al.* [63]. Similarly, Prokhorov and Moraghan [64] reported PSD slopes between 0.5 and 0.8 for their sample. Meyer *et al.* [65] investigated 9.5 years of weekly binned *Fermi*-LAT data for six FSRQs and found flatter PSD slopes in the range 0.65 to 1.1. Among the sources highlighted here, only sources 3C 279 and Mrk 421 are also present in our sample, for which we obtained flatter slopes of 0.80 ± 0.08 and 0.69 ± 0.07, respectively. These comparisons suggest that methodological differences—including the PSD estimation technique (e.g., Fourier transform vs Lomb-Scargle periodogram), binning cadence, and the duration and brightness of light curves—can significantly influence the estimated PSD slopes. Importantly, our use of longer-duration data, including both high- and low-brightness phases and a broader sample of blazars, naturally leads to a wider distribution of slope values.

Binning the data can influence the PSD slope and the distribution of flux values. In our analysis, some sources show log-normality in the three-day binned light curves but not in the seven-day binning (and vice versa). This suggests that the variability mechanisms may operate on different timescales, and binning might highlight or obscure certain behaviors. Binning can smooth out shorter-term variations, which might explain the disappearance of log-normality in certain cases when transitioning to a longer bin. Additionally, the lack of PSD break implies no observed characteristic timescale within the *Fermi* observational window, consistent with a superposition of stochastic events (e.g., shock-in-jet models). Breaks are usually associated with physical processes like cooling or crossing a specific size scale in the jet or emission region. The lack of such breaks indicates continuous variability without a dominant timescale.

The spectral index distribution analysis of BL Lac and FSRQ sources over different binning intervals reveals the complexity of the underlying variability processes in these sources. While normality was accepted in select cases, the prevalence of log-normal/double log-normal fits suggests a more intricate spectral index distribution. This observation aligns with the idea that blazar variability is often nonlinear and multimodel, which is consistent with other studies showing that blazars exhibit flux variations across different timescales driven by stochastic processes in the relativistic jets. The higher reduced-χ^2 values for sources like 4FGL $1104.4+3812$ and 4FGL $2158.8-3013$ indicate that even double log-normal models may not capture all the variability, hinting at the possible presence of additional physical mechanisms or more complex emission models that govern the spectral behavior of these sources. This calls for the application of more sophisticated statistical models to better characterize the spectral index distributions, particularly when examining longer-timescale variability in blazars. Understanding the longer variability patterns is crucial for refining theoretical models of blazar emission and improving predictions of their variability patterns across different energy bands.

VIII. CONCLUSION

This comprehensive study of long-term *Fermi*-LAT γ-ray light curves for a large sample of blazars (FSRQs, BL Lacs, and BCUs) across multiple time binnings (three-day, seven-day, and 30-day) reveals that variability characteristics depend strongly on both blazar subclass and observational timescale. FSRQs consistently show higher fractional variability (F_{var}) than BL Lacs and BCUs, supporting the view that their powerful jets and high accretion rates drive stronger flux variations. BCUs display intermediate behavior, often resembling BL Lacs in variability amplitude. The correlation between γ-ray flux and spectral index shows that BL Lacs and BCUs generally follow a softer when brighter trend, indicative of cooling-dominated processes, while FSRQs exhibit a slight "harder when brighter" trend, especially at longer time bins, hinting at different acceleration or emission mechanisms. The lack of flux-index correlation in FSRQs at shorter time bins suggests that short-term flares may obscure underlying long-term processes. Log-normal flux distributions, observed in many sources across all time bins, point to multiplicative variability processes likely tied to turbulent accretion flows or jet dynamics. Their persistence across timescales suggests such processes operate over a broad temporal range. The appearance of bimodal or double-log-normal distributions in some blazars indicates distinct variability states or multiple overlapping multiplicative processes. Positive correlations between bimodal centroids imply coherent flux changes across states, while negative correlations between distribution widths—especially in BL Lacs—suggest reduced variability during specific activity phases. FSRQs, in contrast, show consistent positive correlations across multiple parameters, indicating more structured variability. PSD analysis reveals a wide diversity of slopes, reflecting variability across a broad range of timescales. BL Lacs typically show flatter PSD slopes (< 1), particularly in three-day bins, while FSRQs tend to exhibit steeper slopes—especially in seven-day bins—indicating more

structured, red-noise-like behavior. The flatter slopes reported here, compared to earlier studies, align with more recent long-term monitoring and suggest that variability characteristics evolve with extended observations. Differences across studies likely arise from variations in binning cadence, PSD estimation methods, and inclusion of diverse brightness states. Overall, these results highlight the importance of long-duration, multitimescale monitoring to unravel the physical mechanisms driving blazar variability and to better understand their jet dynamics and central engines.

ACKNOWLEDGMENTS

Z. S. is supported by the Department of Science and Technology, Government of India, under the INSPIRE Faculty Grant No. DST/INSPIRE/04/2020/002319. We express gratitude to the *Fermi*-LAT for providing a comprehensive long-term γ-ray data of high-energy sources.

DATA AVAILABILITY

The data that support the findings of this article are openly available [26].

[1] W. B. Atwood *et al.*, Astrophys. J. **697**, 1071 (2009).
[2] S. Abdollahi *et al.*, Astrophys. J. Suppl. Ser. **260**, 53 (2022).
[3] A. A. Abdo *et al.* (Fermi LAT Collaboration), Astrophys. J. Suppl. Ser. **188**, 405 (2010).
[4] C. M. Urry and P. Padovani, Publ. Astron. Soc. Pac. **107**, 803 (1995).
[5] R. Blandford, D. Meier, and A. Readhead, Annu. Rev. Astron. Astrophys. **57**, 467 (2019).
[6] J. Albert *et al.*, Astrophys. J. Lett. **666**, L17 (2007).
[7] M. Ackermann *et al.*, Astrophys. J. Lett. **824**, L20 (2016).
[8] M.-H. Ulrich, L. Maraschi, and C. M. Urry, Annu. Rev. Astron. Astrophys. **35**, 445 (1997).
[9] *Blazar Variability Workshop II: Entering the GLAST Era*, edited by H. R. Miller, K. Marshall, J. R. Webb, and M. F. Aller, Astronomical Society of the Pacific Conference Series Vol. 350 (2006).
[10] A. A. Abdo *et al.*, Astrophys. J. **700**, 597 (2009).
[11] A. A. Abdo *et al.*, Astrophys. J. **716**, 30 (2010).
[12] M. Böttcher, A. Reimer, K. Sweeney, and A. Prakash, Astrophys. J. **768**, 54 (2013).
[13] Z. Shah, S. Sahayanathan, N. Mankuzhiyil, P. Kushwaha, R. Misra, and N. Iqbal, Mon. Not. R. Astron. Soc. **470**, 3283 (2017).
[14] Z. Shah, V. Jithesh, S. Sahayanathan, and N. Iqbal, Mon. Not. R. Astron. Soc. **504**, 416 (2021).
[15] Z. Shah, Mon. Not. R. Astron. Soc. **527**, 5140 (2024).
[16] A. Mücke and R. J. Protheroe, Astropart. Phys. **15**, 121 (2001).
[17] I. G. Kramarenko, A. B. Pushkarev, Y. Y. Kovalev, M. L. Lister, T. Hovatta, and T. Savolainen, Mon. Not. R. Astron. Soc. **510**, 469 (2021).
[18] M. Hayashida *et al.*, Astrophys. J. **754**, 114 (2012).
[19] M. Hayashida *et al.*, Astrophys. J. **807**, 79 (2015).
[20] M. Ackermann *et al.*, Astrophys. J. Lett. **813**, L41 (2015).
[21] E. W. Bonning, C. Bailyn, C. M. Urry, M. Buxton, G. Fossati, L. Maraschi, P. Coppi, R. Scalzo, J. Isler, and A. Kaptur, Astrophys. J. Lett. **697**, L81 (2009).
[22] Z. Shah, V. Jithesh, S. Sahayanathan, R. Misra, and N. Iqbal, Mon. Not. R. Astron. Soc. **484**, 3168 (2019).
[23] S. Akbar, Z. Shah, R. Misra, and N. Iqbal, Astrophys. J. **977**, 111 (2024).
[24] J. Tantry, Z. Shah, R. Misra, N. Iqbal, and S. Akbar, J. High Energy Astrophys. **44**, 393 (2024).
[25] S. Li, Z.-Q. Xia, Y.-F. Liang, N.-H. Liao, and Y.-Z. Fan, Astrophys. J. **853**, 159 (2018).
[26] S. Abdollahi *et al.*, Astrophys. J. Suppl. Ser. **265**, 31 (2023).
[27] A. A. Abdo *et al.*, Astrophys. J. **707**, 1310 (2009).
[28] J. Ballet, T. H. Burnett, S. W. Digel, and B. Lott, Astrophys. J. Suppl. Ser. **247**, 33 (2020).
[29] S. Abdollahi *et al.*, Astrophys. J. Suppl. Ser. **265**, 31 (2023).
[30] S. Vaughan, R. Edelson, R. S. Warwick, and P. Uttley, Mon. Not. R. Astron. Soc. **345**, 1271 (2003).
[31] B. Schleicher *et al.*, Galaxies **7**, 62 (2019).
[32] Z. Shah, N. Mankuzhiyil, A. Sinha, R. Misra, S. Sahayanathan, and N. Iqbal, Res, Astron. Astrophys. **18**, 141 (2018).
[33] Z. Shah, R. Misra, and A. Sinha, Mon. Not. R. Astron. Soc. **496**, 3348 (2020).
[34] R. Khatoon, Z. Shah, R. Misra, and R. Gogoi, Mon. Not. R. Astron. Soc. **491**, 1934 (2020).
[35] M. Ackermann *et al.*, Astrophys. J. **743**, 171 (2011).
[36] A. Paggi, A. Cavaliere, V. Vittorini, F. D'Ammando, and M. Tavani, Astrophys. J. **736**, 128 (2011).
[37] B. Rajput, C. S. Stalin, and S. Rakshit, Astron. Astrophys. **634**, A80 (2020).
[38] G. Ghisellini, F. Tavecchio, L. Foschini, and G. Ghirlanda, Mon. Not. R. Astron. Soc. **414**, 2674 (2011).
[39] L. Foschini, G. Ghisellini, F. Tavecchio, G. Bonnoli, and A. Stamerra, Astron. Astrophys. **530**, A77 (2011).
[40] G. Ghisellini and F. Tavecchio, Mon. Not. R. Astron. Soc. **397**, 985 (2009).
[41] M. Ackermann *et al.*, Astrophys. J. **741**, 30 (2011).
[42] G. G. Madejski and M. Sikora, Annu. Rev. Astron. Astrophys. **54**, 725 (2016).
[43] R. de Menezes, R. A. Amaya-Almazán, E. J. Marchesini, H. A. Peña-Herazo, F. Massaro, V. Chavushyan, A. Paggi, M. Landoni, N. Masetti, F. Ricci, R. D'Abrusco, F. La Franca, H. A. Smith, D. Milisavljevic, G. Tosti, E. Jiménez-Bailón, and C. C. Cheung, Astrophys. J. Suppl. Ser. **365**, 12 (2020).
[44] N. Álvarez Crespo, F. Massaro, R. D'Abrusco, M. Landoni, N. Masetti, V. Chavushyan, E. Jiménez-Bailón, F. La Franca, D. Milisavljevic, A. Paggi, V. Patiño-Álvarez,

F. Ricci, and H. A. Smith, Astrophys. J. Suppl. Ser. **361**, 316 (2016).
[45] G. Chiaro, D. Salvetti, G. La Mura, M. Giroletti, D. J. Thompson, and D. Bastieri, Mon. Not. R. Astron. Soc. **462**, 3180 (2016).
[46] J. Lefaucheur and S. Pita, Astron. Astrophys. **602**, A86 (2017).
[47] S. Scaringi, E. Körding, P. Uttley, C. Knigge, P. J. Groot, and M. Still, Mon. Not. R. Astron. Soc. **421**, 2854 (2012).
[48] Y. E. Lyubarskii, Mon. Not. R. Astron. Soc. **292**, 679 (1997).
[49] P. Uttley, I. M. McHardy, and S. Vaughan, Mon. Not. R. Astron. Soc. **359**, 345 (2005).
[50] I. McHardy, in *The Jet Paradigm. Lecture Notes in Physics*, edited by T. Belloni (Springer, Berlin, Heidelberg, 2010), Vol. 794, p. 203.
[51] M. Péault, J. Malzac, M. Coriat, T. D. Russell, K. I. I. Koljonen, R. Belmont, S. Corbel, S. Drappeau, J. Ferreira, P. O. Petrucci, J. Rodriguez, and D. M. Russell, Mon. Not. R. Astron. Soc. **482**, 2447 (2019).
[52] A. Kundu, R. Chatterjee, K. Mitra, and S. Mondal, Mon. Not. R. Astron. Soc. **510**, 3688 (2022).
[53] J. A. Gaidos *et al.*, Nature (London) **383**, 319 (1996).
[54] F. Aharonian *et al.*, Astrophys. J. Lett. **664**, L71 (2007).
[55] R. Narayan and T. Piran, Mon. Not. R. Astron. Soc. **420**, 604 (2012).
[56] A. Sinha, R. Khatoon, R. Misra, S. Sahayanathan, S. Mandal, R. Gogoi, and N. Bhatt, Mon. Not. R. Astron. Soc. **480**, L116 (2018).
[57] J. Biteau and B. Giebels, Astron. Astrophys. **548**, A123 (2012).
[58] A. A. Abdo *et al.*, Astrophys. J. **722**, 520 (2010).
[59] R. Chatterjee, C. D. Bailyn, E. W. Bonning, M. Buxton, P. Coppi, G. Fossati, J. Isler, L. Maraschi, and C. M. Urry, Astrophys. J. **749**, 191 (2012).
[60] M. A. Sobolewska, A. Siemiginowska, B. C. Kelly, and K. Nalewajko, Astrophys. J. **786**, 143 (2014).
[61] K. Nakagawa and M. Mori, Astrophys. J. **773**, 177 (2013).
[62] P. Kushwaha, A. Sinha, R. Misra, K. P. Singh, and E. M. de Gouveia Dal Pino, Astrophys. J. **849**, 138 (2017).
[63] M. Tarnopolski, N. Żywucka, V. Marchenko, and J. Pascual-Granado, Astrophys. J. Suppl. Ser. **250**, 1 (2020).
[64] D. A. Prokhorov and A. Moraghan, Mon. Not. R. Astron. Soc. **471**, 3036 (2017).
[65] M. Meyer, J. D. Scargle, and R. D. Blandford, Astrophys. J. **877**, 39 (2019).